THE JOURNAL OF PHYSICAL CHEMISTRY C

Article

pubs.acs.org/JPCC

Influence of the Excited-State Charge-Transfer Character on the Exciton Dissociation in Donor−Acceptor Copolymers

Katharina Neumann,[†] Christian Schwarz,[‡] Anna Köhler,[‡] and Mukundan Thelakkat*,[†]

[†]Applied Functional Polymers, Macromolecular Chemistry I, University of Bayreuth, 95440 Bayreuth, Germany

[‡]Experimental Physics II and Bayreuth Institute of Macromolecular Research (BIMF), University of Bayreuth, 95440 Bayreuth, Germany

Supporting Information

ABSTRACT: We synthesize a polytriphenylamine homopolymer and two donor−acceptor copolymers (D−A-copolymers) based on triphenylamine (TPA) as donor in combination with two different acceptor moieties to study the effect of the acceptor unit on the excited-state charge-transfer characteristics (CT-characteristics) and charge separation. The two acceptor moieties are a dicyanovinyl group in the side chain and a thieno[3,4-*b*]thiophene carboxylate in the main chain. Absorption and photoluminescence studies show new CT-bands for both of the D−A-copolymers. Field-dependent charge extraction studies in bilayer solar cells indicate a stronger CT-character for the copolymer in which the acceptor group is less conjugated with the copolymer backbone. The D−A-copolymer carrying the acceptor unit in the main chain exhibits smaller excitonic CT-character and good conjugation leading to less-bound electron−hole pairs and a better charge separation. This fundamental study gives insight into the interdependence of conjugation, charge carrier mobility, and solar cell performance for two different D−A-copolymers.

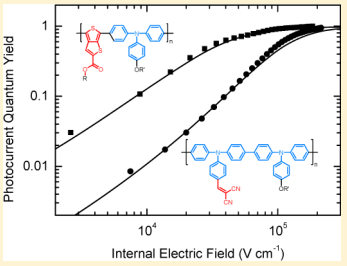

1. INTRODUCTION

There is intensive research in the field of bulk heterojunction solar cells comprising alternating donor−acceptor copolymers (D−A-copolymers) and fullerene derivatives with the aim to design novel D−A-copolymers and thus to increase the power conversion efficiency.[1−3] In general, two strategies are widely used as the design principle for these D−A-copolymers: (a) introduction of the A unit as a side chain on the donor backbone and (b) incorporation of D and A in the main chain to get alternating D−A-copolymers.[4−10] The diverse elementary processes and dynamics of charge transfer (CT) and charge separation in such a bulk heterojunction solar cell have been intensively studied.[11,12] After light absorption a bound metastable intermolecular CT-state is formed by electron transfer to a neighboring molecule. This state can separate into free charge carriers or recombine. Since the charge separation is a key step, it is very important to understand the influence of conjugation and excited-state CT-character on this process. Commonly, the CT-character of the excited state between D−A-copolymer and fullerene acceptor has been investigated.[13] It is equally important to understand and correlate the degree of excited-state CT-character of the D−A-copolymer itself with its charge carrier mobility as well as the charge separation with fullerenes. It was shown by Tautz et al. that the polaron pair yield in D−A-copolymers is dependent on the electron affinity of the acceptor moiety.[14] A correlation of this observation with charge separation and device characteristics was not reported there. Furthermore, Carsten et al. showed that not only the energetics but also the internal dipole moment along the polymer chain may be critical for the CT-state, and these results were compared with charge separation in bulk heterojunction devices.[15] Here, we first correlate the observed CT-character with the conjugation/delocalization as well as with the charge carrier mobility in the D−A-polymer itself. The observed CT-character is then compared with the charge separation in fullerene bilayer devices. We selected a well-defined bilayer device to avoid possible morphological differences in blend devices on using different polymers. Our material system consists of two novel D−A-copolymers based on triphenylamine (TPA). We chose a system containing TPA which is a widely examined and well-known donor material with excellent thermal and electrochemical stability.[16] The CT-character of the excited state of D−A-copolymers depends on the nature of attachment of the acceptor unit to the donor moiety. Here, we compare two different D−A-copolymers: (a) with a dicyanovinyl acceptor in the side chain (**P2**) and (b) with a thieno[3,4-*b*]thiophene acceptor in the main chain (**P3**) with the homopolymer (**P1**) without any acceptor unit. Since the resulting interaction between electron donating and the electron withdrawing molecules usually leads to the formation of an intramolecular CT-state,[17] the two different strategies adopted here can result in different degrees of CT-character and conjugation or delocalization between the D and A moieties.

2. EXPERIMENTAL SECTION

2.1. Synthesis and Polymerization. **P1**: 4-Bromo-*N*-(4-bromophenyl)-*N*-(4-(2-ethylhexyloxy)phenyl)aniline (**1**; 516

Received: July 16, 2013
Revised: December 5, 2013

   dx.doi.org/10.1021/jp407014q | *J. Phys. Chem. C* XXXX, XXX, XXX−XXX

mg, 0.97 mmol) and 4-(2-ethylhexyloxy)-*N*,*N*-bis(4-(4,4,5,5-tetramethyl-1,3,2-dioxaborolan-2-yl)phenyl)aniline (**2**; 607 mg, 0.972 mmol) were dissolved in 8 mL of tetrahydrofuran (THF). A 5.3 mL aliquot of 2 M K_2CO_3 in water and dimethylformamide (DMF; 1:1) were added, and the mixture was purged with argon for 30 min. $Pd(PPh_3)_4$ (45 mg, 0.04 mmol) and $Pd(OAc)_2$ (4 mg, 0.02 mmol) were added, and the reaction mixture was heated to 70 °C. After 72 h the polymerization was end-capped by the addition of phenylboronic acid pinacol ester and bromobenzene for 3 h. After cooling, the reaction mixture was extracted with dichloromethane (DCM) and water. The crude product poly[*N*,*N*′-bis(4-(2-ethylhexyloxy)phenyl)-*N*,*N*′-di-*p*-tolylbiphenyl-4,4′-diamine] (**P1**) was precipitated in MeOH and purified by sequential Soxhlet extraction in MeOH and EtOH. Yield: 66%. ^{1}H NMR (300 MHz, $CDCl_3$, 298 K; ppm): δ 7.51−7.36 (d, 2H, H_{ar}), 7.18−6.99 (d, 2H, H_{ar}), 6.93−6.81 (m, 6H, H_{ar}), 3.83 (d, 2H, O−CH_2), 1.80−1.66 (m, 1H, CH), 1.60−1.39 (m, 8H, CH_2), 1.34 (s, 12 H, CH_3), 0.97−0.84 (m, 6H, CH_3).

P2: First, an aldehyde functionalized copolymer was synthesized as precursor. For that, 4-(bis(4-bromophenyl)-amino)benzaldehyde (0.79 g, 1.83 mmol) and **2** (1.15 g, 1.83 mmol) were dissolved in 15 mL of THF. After addition of 2.33 mL of 2 M K_2CO_3 in water and DMF (1:1), the mixture was degassed. A 20 mg (0.017 mmol) amount of $Pd(PPh_3)_4$ and 2 mg (0.009 mmol) of $Pd(OAc)_2$ were added, and the reaction mixture was heated to 70 °C. After 5 days, phenylboronic acid pinacol ester and bromobenzene were added for end-capping and the mixture was stirred for 3 h. The reaction mixture was cooled to room temperature and extracted with dichloromethane (DCM) and brine. The organic phase was dried over Na_2SO_4, and the solvent was evaporated under reduced pressure. The dark brown residue was dissolved in THF, and a small amount of the scavenger *N*,*N*-diethylphenylazothioformamide was added. After 3 h at room temperature the polymer was precipitated in MeOH followed by a Soxhlet extraction in EtOH for 12 h. Poly[4-((4′-((4-(2-ethylhexyloxy)phenyl)(*p*-tolyl)amino)biphenyl-4-yl)(*p*-tolyl)-amino)benzaldehyde] was obtained as beige powder. Yield: 70%. ^{1}H NMR (300 MHz, $CDCl_3$, 298 K; ppm): δ 9.83 (s, 1H, CHO), 7.84−7.64 (s, 2H, H_{ar}), 7.64−7.34 (m, 4H, H_{ar}), 7.23−6.95 (m, H_{ar}), 6.95−6.64 (s, H_{ar}), 3.93−3.67 (d, 2H, O−CH_2), 1.85−1.62 (m, 1H, CH), 1.59−1.37 (m, 8H, CH_2), 1.34 (s, 12H, CH_3), 0.91 (s, 6H, CH_3). IR (cm^{-1}): ν 2915 (s), 2842 (s), 1692 (m), 1588 (m), 1488 (m), 1469 (s), 1263 (m), 1161 (m), 1109 (m), 816 (m), 718 (s).

Second, the precursor copolymer poly[4-((4′-((4-(2-ethylhexyloxy)phenyl)(*p*-tolyl)amino)biphenyl-4-yl)(*p*-tolyl)-amino)benzaldehyde] (736 mg, 1.14 mmol) was dissolved in 9 mL of pyridine and 2 mL of acetic acid. After purging with argon for 30 min, malonodinitrile (2 mg, 0.24 mmol) and one crystal of NH_4OAc were added and the solution was stirred for 70 h at room temperature. The reaction mixture was extracted with DCM and water. The organic phase was washed with water and dried over Na_2SO_4. After evaporation of the solvent under reduced pressure, the polymer was precipitated from THF in MeOH. 2-(4-((4′-((4-(2-Ethylhexyloxy)phenyl)(*p*-tolyl)amino)biphenyl-4-yl)(*p*-tolyl)amino)benzylidene)-malonodinitrile (**P2**) was obtained as dark red powder. Yield: 98%. ^{1}H NMR (300 MHz, $CDCl_3$, 298 K; ppm): δ 7.87−7.67 (m, 2H, H_{ar}), 7.56 (s, 1H, H_{vinyl}), 7.52−7.33 (m, 4H, H_{ar}), 7.20−6.92 (m, 10H, H_{ar}), 6.92−6.56 (m, 2H, H_{ar}), 3.93−3.67 (d, 2H, OCH_2), 1.81−1.58 (m, 1H, CH), 1.58−1.37 (m, 8H, CH_2), 0.95−0.73 (m, 6H, CH_3). IR [cm^{-1}]: ν 2927 (m), 2222 (m), 1567 (m), 1487 (s), 1237 (m), 1181 (m), 1112 (m), 817 (s), 696 (m).

P3: Compound **2** (590 mg, 0.94 mmol) and 4-bromothiophene-3-carbaldehyde (**4**; 429 mg, 0.94 mmol) were dissolved in 8 mL of THF. A 5 mL aliquot of 2 M K_2CO_3 in water and DMF (1:1) were added, and the mixture was purged with argon for 30 min. Then $Pd(PPh_3)_4$ (22 mg, 0.02 mmol) and $Pd(OAc)_2$ (2 mg, 0.01 mmol) were added, and the reaction mixture was heated to 70 °C in a microwave. After 5 h the reaction mixture was extracted with DCM and water. The crude product poly[octyl-6-(4-((4-(2-ethylhexyloxy)-phenyl)(*p*-tolyl)amino)phenyl)-*alt*-4-octylthieno[3,4-*b*]-thiophene-2-carboxylate] (**P3**) was precipitated in MeOH and purified by Soxhlet extraction in EtOH and acetone. Yield: 40%. ^{1}H NMR (300 MHz, $CDCl_3$, 298 K; ppm): δ 8.06−7.87 (s, 1H, H_{ar}), 7.68−7.40 (m, 4H, H_{ar}), 7.25−7.02 (m, 6H, H_{ar}), 7.02−6.72 (m, 2H, H_{ar}), 4.47−4.19 (d, 2H, OCH_2), 4.02−3.72 (d, 2H, OCH_2), 1.88−1.68 (m, 1H, CH), 1.68−1.12 (m, 26H, CH_2), 1.10−0.72 (m, 9H, CH_3).

2.2. Physical Measurements. Number-average (M_n) and weight-average (M_w) molecular weights were determined by size exclusion chromatography (SEC) using a Waters 515-HPLC pump with stabilized THF as the eluent. The flow rate was 0.5 mL min^{-1}. The column setup consisted of a guard column (Varian; 50 × 0.75 cm; ResiPore; particle size, 3 μm) and two separation columns (Varian; 300 × 0.75 cm; ResiPore; particle size, 3 μm). The compounds were monitored with a Waters UV detector at 254 nm. SEC in chlorobenzene was carried out at 60 °C on an Agilent 1100 series SEC using two Polymer Laboratories mixed B columns. Both SEC systems were calibrated against polystyrene. Thermogravimetric analysis (TGA) measurements were carried out using a Mettler Toledo TGA/SDTA 851^e with a heating rate of 40 °C min^{-1} under nitrogen flow, and the temperature of degradation (T_d) corresponds to a 5% weight loss. Differential scanning calorimetry (DSC) analysis was performed on a Perkin-Elmer Diamond differential scanning calorimeter, calibrated with indium. Glass transition temperature (T_g) was determined using a scanning rate of 20 °C min^{-1} under a nitrogen flow.

Cyclic voltammograms (CVs) were recorded under moisture- and oxygen-free conditions using a standard three-electrode assembly connected to a potentiostat (model 263A, EG&G Princeton Applied Research) and at a scanning rate of 50 mV s^{-1}. The working electrode was a glassy carbon disk electrode (area, $^1/_4 \times 0.0314$ cm^2), a platinum wire was used as auxiliary electrode, and the quasi-reference electrode was Ag/Ag^+ composed of a Ag wire and $AgNO_3$ in acetonitrile. Tetrabutylammonium hexafluorophosphate (Bu_4NPF_6, 0.1 M) was used as the conducting salt. Each measurement was calibrated with an internal standard (ferrocene/ferrocenium). The HOMO values were determined from the value of −5.16 eV for ferrocene with respect to vacuum level and correcting for the solvent effects.

For spectroscopic measurements polymer films were spin-coated from filtered chlorobenzene solutions (10 mg mL^{-1}). Solution measurements were also performed in chlorobenzene with a concentration of the repetition units of 10^{-5}−10^{-3} mol L^{-1}. Absorption was measured with a Cary 5000 (Varian) UV−vis spectrometer. The fluorescence quantum yields were measured in an integration sphere filled with nitrogen under illumination with an Ar^+ laser (**P1**, UV-multiline 351 nm/364 nm; **P2** and **P3**, 488 nm) with a charge-coupled-device (CCD)

dx.doi.org/10.1021/jp407014q | J. Phys. Chem. C XXXX, XXX, XXX−XXX

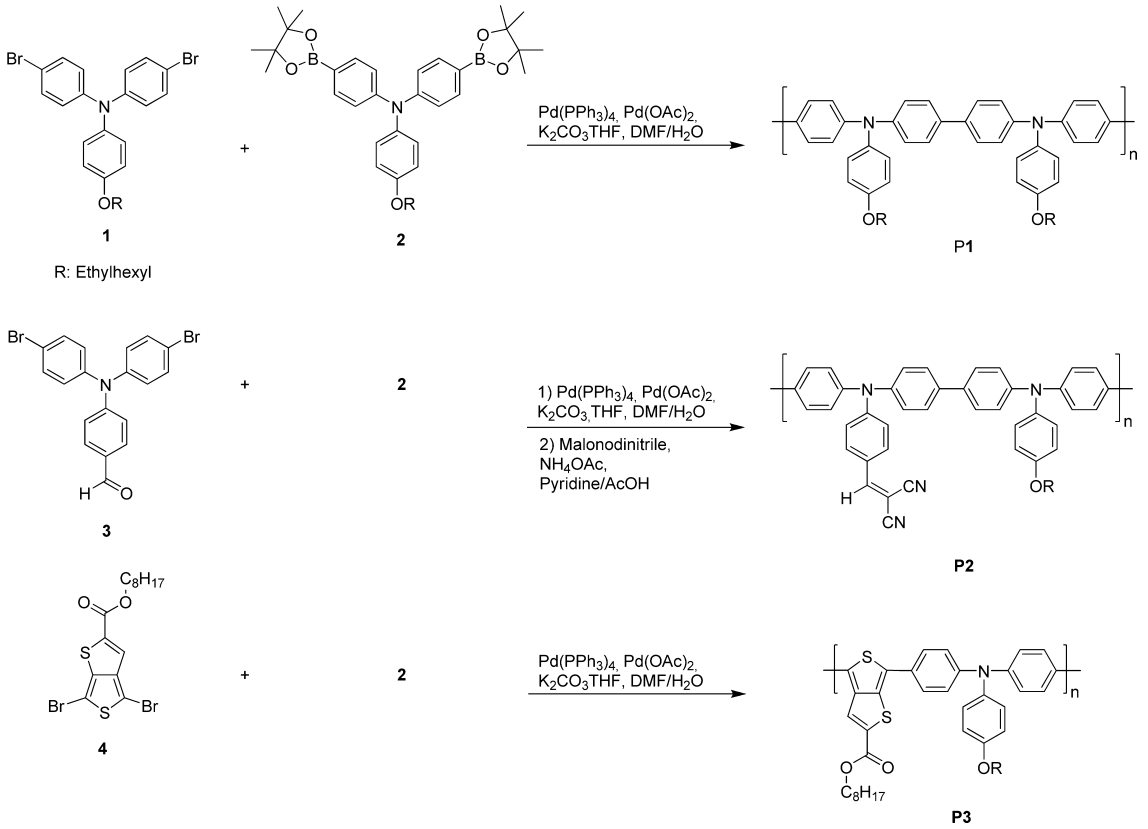

Figure 1. Scheme of the syntheses of polymers **P1**, **P2**, and **P3** via Suzuki polycondensation. The bis-boronic ester monomer **2** was reacted with the three different dibrominated monomers **1**, **3**, and **4**. The polycondensation of **P3** was carried out under microwave irradiation.

camera as described elsewhere.[18] The fluorescence spectra were recorded on a time-correlated single photon counting (TCSPC) setup at room temperature with the samples in vacuum under excitation from a laser diode (**P1**, 375 nm; **P2** and **P3**, 485 nm).

Electric devices were fabricated on structured ITO-coated glass substrates using AZ 1518 photopaint from Microchemicals to define the active area and to prevent edge effects. The devices were then plasma-edged, and a 50 nm layer of poly(3,4-ethylenedioxythiophene):poly(styrene-sulfonate) (PEDOT:PSS; Clevios) was spin-coated into the active area. The PEDOT:PSS layer was heated to 180 °C for 30 min, followed by spin-coating a 40 nm polymer layer on top of it for the bilayer solar cells. Then a 40 nm C_{60} layer (99.9% purity, American Dye Source Inc.) and a 100 nm aluminum layer were evaporated at 5×10^{-7} mbar. For the space−charge-limited current (SCLC) devices, the polymers were blade-coated from chlorobenzene solutions and a 40 nm gold electrode was evaporated.

All device measurements were performed under active vacuum at room temperature with a Keithley source measure unit. For performance and field-dependent measurements a Newport 1.5 AM solar simulator was used, and the solar spectrum measurements were recorded under monochromatic illumination of a 150 W xenon lamp. Light intensities were recorded with a Hamamatsu S1337-33BQ photodiode. The internal field F was calculated as $F = (V_{oc} - V)/d$ with applied external voltage V, the open-circuit voltage V_{oc}, and the active film thickness d.

3. RESULTS

3.1. Synthesis. Here, we present the synthesis and characterization of a main chain homopolymer (**P1**, poly[*N*,*N*′-bis(4-(2-ethylhexyloxy)phenyl)-*N*,*N*′-di-*p*-tolylbiphenyl-4,4′-diamine]), an alternating D−A-copolymer with dicyanovinyl in the side chain (**P2**, poly[2-(4-((4′-((4-(2-ethylhexyloxy)phenyl)(*p*-tolyl)amino)biphenyl-4-yl)-*alt*-(*p*-tolyl)amino)benzylidene)malononitrile]) and the D−A-copolymer carrying thieno[3,4-*b*]thiophene-2-carboxylate in the main chain (**P3**, poly[octyl-6-(4-((4-(2-ethylhexyloxy)phenyl)(*p*-tolyl)amino)phenyl)-*alt*-4-octylthieno[3,4-*b*]thiophene-2-carboxylate]. The dicyanovinyl group is strongly electron withdrawing. It has been shown that the introduction of this group as a side chain lowers the optical gap, by mainly lowering the LUMO value.[10] On the other hand, the electron withdrawing comonomer thieno[3,4-*b*]thiophene carboxylate stabilizes the quinoidal form and therefore lowers the optical gap when coupled with a suitable donor comonomer.[19,20] We used Suzuki AA/BB type polycondensation as a synthetic method to obtain the conjugated polymers[21] because it enables the synthesis of well-defined alternating copolymers. The symmetrically difunctionalized monomers were synthesized according to the literature with good yields (see the Supporting Information).[22,23]

Homopolymer **P1** was obtained by polycondensation between a dibromo-TPA and a TPA bis-boronic acid ester (Figure 1). The synthesis of **P2** was realized by a precursor method. We used monomer **3**, a dibromo-TPA with an aldehyde group which is stable under Suzuki polycondensation conditions, and polymerized it with the common bis-boronic acid ester monomer **2**. After purifying the precursor copolymer

dx.doi.org/10.1021/jp407014q | J. Phys. Chem. C XXXX, XXX, XXX−XXX

by Soxhlet extraction, the dicyanovinyl group was introduced via a polymer analogous Knoevenagel condensation with malonodinitrile. ^{1}H NMR spectroscopy and FT-IR spectroscopy clearly proved the complete conversion of the aldehyde functionality to the dicyanovinyl group (see the Supporting Information).

The alternating main chain D−A-copolymer **P3** was synthesized by reacting directly the dibromo-monomer thieno[3,4-*b*]thiophene carboxylate **4** with monomer **2** under microwave irradiation. All polymers were soluble in THF, $CHCl_3$, and chlorobenzene, whereas **P3** was soluble only in $CHCl_3$ and chlorobenzene.

3.2. Polymer Properties. M_w and M_n of polymers **P1**, **P2**, and **P3** were determined by SEC with THF as eluent. For calibration a polystyrene standard was used. Copolymer **P3** was analyzed in a chlorobenzene SEC at 60 °C due to the low solubility in THF. Homopolymer **P1** has a M_n of 10330 g mol^{-1} and a M_w of 15770 g mol^{-1}. Both D−A-copolymers show a comparable M_n with 7400 and 7770 g mol^{-1} for **P2** and **P3**, respectively. The corresponding M_w are 18760 g mol^{-1} and 11610 g mol^{-1}, and all of the relevant SEC data are given in Table 1. The homopolymer and all copolymers showed high thermal stability in TGA with temperatures for 5% weight loss ranging from 402 to 410 °C. All of the polymers form optically clear and smooth films, which is advantageous for device preparation. DSC analysis showed that all compounds were amorphous and had glass transition temperatures of 203, 212 and 118 °C for **P1**, **P2**, and **P3**, respectively.

Table 1. Molecular Weights and Thermal Properties of Homopolymer P1 and D−A-Copolymers P2 and P3[a]

polymer	M_n (g mol^{-1})	M_w (g mol^{-1})	PDI	T_d (°C)	T_g (°C)
P1	10330	15770	1.52	402	203
P2	7400	18760	2.54	410	212
P3	7770	11610	4.91	370	118

[a]SEC analysis was carried out in THF as eluent and polystyrene standards at room temperature. **P3** was measured in chlorobenzene at 60 °C.

Cyclic voltammetry measurements were employed to investigate the redox behavior and the influence of the different electron withdrawing groups on the HOMO/LUMO levels. The HOMO values were calculated by calibrating with ferrocene and correcting for solvent effects.[24,25] The polymers were measured in DCM vs $AgNO_3$. **P1** and **P3** have similar oxidation potential values (0.15 V vs Fc), whereas the oxidation potential of **P2** is slightly higher (0.3 V vs Fc). Thus, the calculated HOMO levels are −5.31, −5.45, and −5.30 eV for **P1**, **P2**, and **P3**, respectively. The values are summarized in Table 2. The LUMO levels were estimated from the optical gap (determined from the onset of absorption bands, vide infra) and the HOMO energy values. Due to the slightly lower optical gap of **P3** the LUMO levels of both D−A-copolymers are similar. Thus, the introduction of the strong electron withdrawing dicyanovinyl acceptor unit as substituent reduces the electron richness and delocalization of the TPA main chain, resulting in an increased oxidation potential by about 0.14 V. Additionally, the redox potential is drastically lowered, resulting in low LUMO values. However, the incorporation of the thieno[3,4-b]thiophene acceptor unit in the main chain does not affect the oxidation potential, indicating a similar oxidizability or delocalization of the main chain as in the homopolymer **P1**. This means that the thieno[3,4-*b*]thiophene carboxylate does not withdraw electrons from the TPA moiety but maintains the conjugation between two TPA units resulting in the same oxidation potential for both **P3** and **P1**. This conclusion can be derived from the fact that an individual TPA unit exhibits an oxidation potential of about 0.2 eV higher than that for a dimer in which the TPA units are in conjugation.[16]

A further relevant parameter for semiconductor materials is the charge carrier mobility. We investigated the hole transport mobilities (μ_h) of the three polymers in hole-only diodes using the SCLC method. This method allows the determination of the bulk charge carrier mobility. A PEDOT:PSS-coated ITO electrode and a gold electrode were used to fabricate the devices. In this case, PEDOT:PSS serves as a hole-injecting electrode. Furthermore, the high work function of the gold electrode hinders the injection of electrons but allows for hole collection. Therefore, the transport of the holes is only limited by the charge carrier mobility of the polymer and can be described by the Mott−Gurney eq 1.[26]

$$J = \frac{9}{8}\varepsilon\varepsilon_0\mu_h\frac{V^2}{L^3} \quad (1)$$

According to this equation the current density J is dependent on the permittivity of free space ε_0, the dielectric constant of the polymer ε (assumed to be 3), the charge carrier mobility μ_h, the thickness of the polymer layer L, and the voltage drop across the device V. Assuming ohmic contacts to the injecting electrode, the current is space−charge-limited at high voltages. The measured I−V curves were fitted according to eq 1 to obtain the hole transport mobility μ_h. By recording different active layer thicknesses, the thickness scaling of the space−charge-limited currents was verified. The log−log plots of J vs L and the fits according to the relation $J \sim V^2/L^3$ are illustrated in the Supporting Information. This clearly indicates that the measured current is space−charge-limited. The contact resistance and series resistance were measured in a reference device without a polymer layer, and the corresponding voltage drop V_r was subtracted from the applied voltage. The built-in

Table 2. (a) HOMO Values of P1, P2, and P3 Obtained from Oxidation Potential (E_{ox}) vs Ferrocene in Cyclic Voltammetry Measurements at 50 mV s^{-1} in DCM with 0.1 M Tetrabutylammonium Hexafluorophosphate[a] **and (b) Hole Transport Mobilities (μ_h) Determined by SCLC Measurements in Hole-Only Devices with PEDOT:PSS and Au as Electrodes**[b]

polymer	E_{ox} vs Fc (eV)	HOMO (eV)	E_g (eV)	LUMO (eV)	μ_h (cm^2 V^{-1} s^{-1})
P1	0.15	−5.31	2.97	−2.34	1.4×10^{-4}
P2	0.29	−5.45	2.24	−3.21	7.6×10^{-5}
P3	0.14	−5.30	2.10	−3.20	3.1×10^{-4}

[a]The HOMO value for ferrocene/ferrocenium oxidation in DCM was taken as −5.16 eV.[25] LUMO values were estimated using the onset of absorption (E_g) from UV−vis measurements and corresponding HOMO values. [b]Given values are the average values of three different measured thicknesses.

dx.doi.org/10.1021/jp407014q | J. Phys. Chem. C XXXX, XXX, XXX−XXX

potential V_{bi} for PEDOT:PSS and gold is estimated to be 0 V. Figure 2 gives the half-log plots of J vs V of the three polymers at similar layer thicknesses and the device geometry.

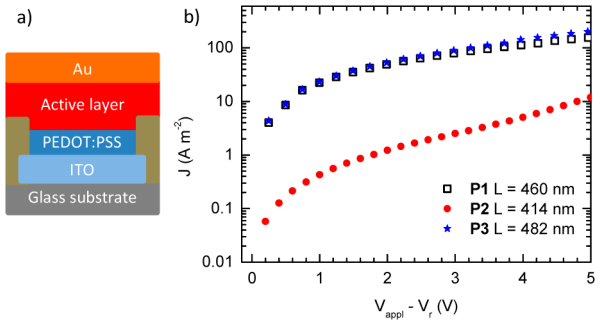

Figure 2. (a) Schematic structure of a hole-only device with PEDOT:PSS and gold as electrodes. (b) Half-log plot of current density J vs voltage V of **P1**, **P2**, and **P3** for comparable layer thicknesses. Additional measurements for different layer thicknesses are given in the Supporting Information.

We found that the homopolymer **P1** shows a hole transport mobility of 1.4×10^{-4} cm^2 V^{-1} s^{-1}. The introduction of the dicyanovinyl groups leads to a decrease of 1 order of magnitude, 7.6×10^{-5} cm^2 V^{-1} s^{-1}, for **P2**. The low mobility of **P2** indicates that the side chain acceptor unit does affect the delocalization or conjugation of the TPA main chain. However, the incorporation of the thieno[3,4-*b*]thiophenecarboxylate does not change the hole transport mobility considerably for **P3** (μ_h = 3.1×10^{-4} cm^2 V^{-1} s^{-1}). These hole transport mobility values are in full agreement with the influence of the acceptor units on the delocalization or the easiness of the oxidation as observed in cyclic voltammetry.

3.3. Absorption and Photoluminescence Spectroscopy. The absorption spectra of **P1**, **P2**, and **P3** in solution and film are shown in Figure 3. We first consider the solution spectra which were recorded at a concentration of the repetition units of 10^{-4} mol L^{-1}. Identical spectra were found at a concentration of 10^{-5} mol L^{-1} with a reduced signal-to-noise ratio. For the homopolymer **P1** we observe an absorption band in the high-energy region centered at 3.22 eV that is characteristic for TPAs and that is assigned to a π–π*-transition. For copolymer **P2** containing the pendant dicyanovinyl group, we find a lower energy absorption peak centered at 2.66 eV with lower oscillator strength that appears in addition to the original TPA absorption band. The latter is blue-shifted by 100 meV to 3.32 eV and has a slightly decreased oscillator strength compared to the homopolymer **P1**. On the basis of the low oscillator strength and low energy, we attribute the 2.66 eV absorption peak present in dilute solution to an intramolecular CT-transition with low wave function overlap from the donor backbone to the dicyanovinyl in the side chain. A similar absorption behavior was also shown for other D–A-copolymers.[10] Overall, the copolymer **P2** is able to cover the whole low- and middle-wavelength region of the visible spectrum.

In **P3**, the thieno[3,4-*b*]thiophene carboxylate, acting as an electron pulling unit, is placed directly in the main chain of the copolymer, allowing for a good electronic interaction with the TPA unit. As for **P2**, we observe a low-energy absorption band centered at 2.49 eV in addition to the original TPA absorption at 3.26 eV. Compared to **P2**, this low-energy band is shifted further to the red by 0.17 eV and carries a higher oscillator strength. Concomitantly, the oscillator strength of the high-energy 3.26 eV band is strongly reduced. We consider the high oscillator strength of the additional, red-shifted absorption peak of **P3** and the reduction of the 3.26 eV intensity to indicate a significant contribution of π–π*-transitions to the intramolecular CT-band that arises from the D–A-type interaction of the electron withdrawing thieno[3,4-*b*]thiophene carboxylate with the TPA unit. Similarly, we interpret the red shift of the low-energy band compared to that of **P2** to indicate a higher degree of conjugation, consistent with a stronger contribution of the delocalized π-orbitals. We obtain the same results for the absorption spectra taken in thin films, except for a small solvent shift. The positions of the absorption peaks are summarized in Table 3.

Table 3. Absorption Peaks (Position of the Center) In a Chlorobenzene Solution at a Concentration of the Repetition Units of 10^{-4} mol L^{-1} and in the Film, Made from Solutions of 10 mg mL^{-1} in Chlorobenzene

polymer	$E_{solution}$ (eV)	E_{film} (eV)
P1	3.22	3.26
P2	2.66, 3.32	2.68, 3.36
P3	2.49, 3.36, 4.11	2.46, 3.34, 4.11

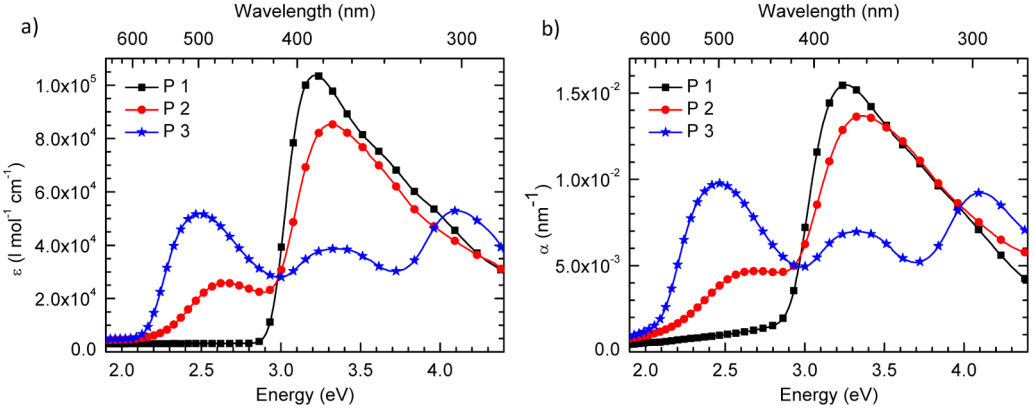

Figure 3. UV–vis absorption spectra of **P1**, **P2**, and **P3**: (a) in chlorobenzene, concentration of the repetition units of 10^{-4} mol L^{-1}; (b) in film from 10 mg mL^{-1} solutions in chlorobenzene.

dx.doi.org/10.1021/jp407014q | J. Phys. Chem. C XXXX, XXX, XXX–XXX

Further information on the nature of excited states in the polymers can be obtained from photoluminescence measurements. First, we find that the three polymers differ strongly in their thin film photoluminescence efficiencies. While integrating sphere measurements taken on thin films give a moderate photoluminescence quantum yield (PL QY) of 3.4% for homopolymer **P1**, the emission is below the detection threshold of this setup for **P2**, and it is as low as 0.7% for **P3**. The uncertainty on the PL QY is about 1%. This trend is consistent with the observed absorption strengths of the lowest energy bands in all three polymers and confirms the indication of a stronger CT-character in **P2** compared to **P3**, and, naturally, of no CT-characteristics in **P1**. Due to the low-emission efficiencies, we used the sensitive technique of TCSPC to measure the photoluminescence spectra and lifetimes. The spectra are shown in Figure 4. No reliable data can be obtained for the spectral window from 2.35 to 2.50 eV due to a technical limitation. Photoluminescence decay curves are included as Supporting Information. We shall discuss the data for the compounds in increasing order of intramolecular CT-character.

For homopolymer **P1**, the same emission band with a 0−0 peak at 2.89 eV and vibronic replica at 2.72 and 2.55 eV is seen in solution and, shifted by 40 meV to the red, in film. This emission dominates for a few nanoseconds after excitation with a lifetime of 0.9 ns in solution and 0.3 ns in the film. At longer times, this emission disappears and a weak, structured emission can be observed. It is shifted to the red by about 0.3 eV and has a lifetime of about 6 ns in solution and 5 ns in film. Since this signal is rather weak with poor spectral to noise ratio, we can spectrally resolve it only for the film, where the higher energy emission decays away fast, yet not for solution. Due to the moderate Stokes's shift of about 0.33 eV between absorption and emission and the concomitant mirror symmetry, we attribute the higher energy emission with 0−0 peak at 2.89 eV to the $\pi-\pi^*$-transition in the TPA-homopolymer, possibly with some mixing of the nonbonding orbital of the nitrogen lone pair. The electronic origin of the lower energy emission at about 2.55 eV is not clear. This emission is present in both phases, solution and film, with the same lifetime, yet in solution it is masked by the stronger higher energy emission. The reduction of the fast component in photoluminescence lifetime in film compared to solution suggests that the weakly red emitting sites can only be populated effectively by energy transfer in the condensed phase of the film.

We next consider the copolymer **P3** where electron-rich and electron-deficient groups alternate in the chain backbone. The spectra in solution and in film immediately after excitation have a spectral shape similar to that in **P1** with similar full width at half-maximum (fwhm) of about 0.2 eV and a comparable Stokes's shift of 0.40 eV. The spectra show a 0−0 peak at 2.10 eV in solution and slightly below, at 2.03 eV, in film. Whereas no spectral change with time is noticeable in solution, in film the higher energy emission decays and exposes a weak emission centered at 1.79 eV that was initially hidden in the red tail of the higher energy peak. The energy difference between the comparatively intense higher energy emission and the weak lower energy emission bands is similar for **P1** and **P3**. In **P1**, it is about 0.30 eV, and in **P3**, it is 0.24 eV. Overall, the dominant decay lifetimes in copolymer **P3** are longer than those of homopolymer **P1**. For **P3** in solution, the decay is not entirely exponential and can best be approximated by a biexponential decay with lifetimes of 2.0 ns (amplitude 20.000) and 3.2 ns

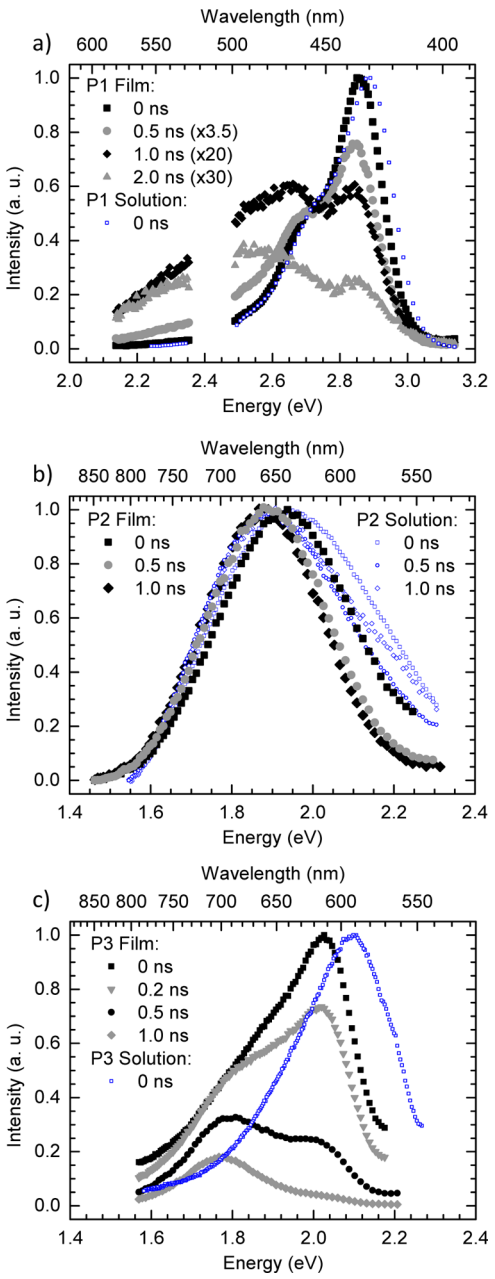

Figure 4. Fluorescence spectra of the polymers in chlorobenzene solutions at a concentration of the repetition units of (**P1** and **P3**, 10^{-5} mol L^{-1}; **P2**, 10^{-3} mol L^{-1}) and in the film under UV-irradiation (**P1**, 375 nm; **P2** and **P3**, 485 nm) measured in a TCSPC setup. In the spectral window from 2.35 to 2.50 eV, no reliable data could be obtained due to a technical limitation.

(amplitude 7.000); i.e., the dominant contribution is twice as long as that for **P1**. This is consistent with the reduced oscillator strength of **P3** compared to **P1** that is also manifested in the intensity of the low-energy absorption peak and the photoluminescence quantum yield. For **P3** in film, the luminescence decay proceeds faster and it is characterized by a distribution of lifetimes.

In contrast to **P1** and **P3**, for **P2** with the dicyanovinyl in the side group we observe a very weak, broad, unstructured emission centered at about 1.9 eV. To enable detection of this inefficiently emitting compound in solution, we used a concentration of the repetition units of 10^{-3} mol L^{-1} instead

dx.doi.org/10.1021/jp407014q | J. Phys. Chem. C XXXX, XXX, XXX−XXX

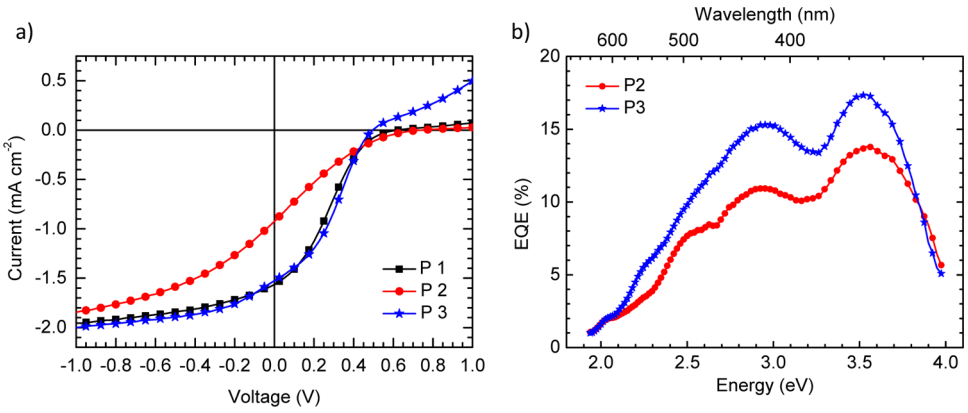

Figure 5. a) Current−voltage characteristics of bilayer solar cells built with the presented polymers **P1**, **P2**, **P3**, and C_{60} under AM 1.5 illumination. (b) Corresponding external quantum efficiency (EQE) spectra of copolymers **P2** and **P3**.

of the 100 times lower value used for **P1** and **P3**. For both, solution and film, the emission does not change with time except for an initial slight red shift that is common for condensed media where spectral diffusion in the density of states prevails.[27] We stress that, in particular, in contrast to **P1** and **P3**, there is no significant change of the spectral shape over time. The emission is characterized by a distribution of lifetimes in the nanosecond range, with more longer lived contributions for the film. Such a broad, unstructured weak emission with a distribution of lifetimes is a general signature for a CT-type transition.

The overall picture that emerges from the absorption and photoluminescence spectroscopy is that, in **P2**, the excited state is dominated by CT-character, manifested in weak absorption and weak, unstructured emission. The homopolymer **P1** shows the moderately intense emission and good absorption associated with $\pi-\pi^*$-transitions as well as a weak, lower energy emission of unclear origin. The nature of the first excited state in the copolymer **P3** lies between the two limiting cases defined by **P1** and **P2**.

3.4. Photocurrent Measurements. We next consider how the different nature of the excited states impacts on their performance as solar cell materials. Therefore, we built bilayer solar cells where C_{60} is evaporated on top of a spin-coated polymer film. Indium−tin-oxide covered by a layer of PEDOT:PSS was used as anode and aluminum as a cathode. The simple device geometry of a bilayer allows for spatially distinct electron and hole pathways to the electrodes, thus preventing the nongeminate recombination of accidentally meeting charge carriers that is inherently problematic in the intermingled morphology of blends. The observed photocurrent characteristics in a bilayer structure can therefore be interpreted as arising mainly from the charge generation at the D−A-interface itself. The current−voltage curves of the bilayer solar cells for the different materials under AM 1.5 illumination are shown in Figure 5, along with the external quantum efficiency (EQE) spectra. The resulting solar cell parameters are given in the Supporting Information.

Homopolymer **P1** and copolymer **P3** show nearly identical current−voltage ($I-V$) curves up to the open-circuit voltage V_{oc}, with similarly moderate performance. The moderate performance is expected for bilayer cells with such material combination.[10] Copolymer **P2** that has the stronger CT-character, however, is distinct and displays a reduced short-circuit current I_{sc} and a concomitantly reduced fill factor FF. The lower efficiency of **P2** compared to **P3** over the whole spectral range is also evident in the EQE spectra that largely follow the absorption data of the blend. All three cells have a pronounced "S-shape", i.e., a zero or low photocurrent for forward bias, at voltages exceeding the open-circuit voltage. The appearance of low current upon further voltage increase is occasionally reported, and it is tentatively attributed to imbalanced mobilities of the donor and the acceptor in planar heterojunction cells.[28]

4. DISCUSSION

The aim of our study is to understand what controls charge separation in D−A-copolymers **P2** and **P3**. The impacts both of dipolar or electrostatic effects and of excited-state delocalization have been demonstrated to be of importance.[29−32] Here, we try to differentiate between both influences by comparing a homopolymer to two D−A-copolymers that represent two different chemical architectures. D−A-copolymer **P2** with a dicyanovinyl group in the side chain (with reduced delocalization with the main chain) shows a stronger CT-character than **P3** where the acceptor moiety is incorporated in the main chain. This is evident from the reduced oscillator strengths of the first absorption band in **P2** compared to **P1** and a barely detectable, broad, unstructured fluorescence that decays nonexponentially. D−A-copolymer **P3** possesses a weaker CT-character as demonstrated by the absorption and photoluminescence properties (vide supra); this results in a lower prominence of the intrachain CT-character due to significant contributions of delocalized π- and π^*-orbitals. The question in now whether the more dipolar character of **P2** favors charge separation, e.g., by preseparation of the hole and electron on the copolymer and concomitant dielectric screening,[29] or whether the higher degree of excited-state delocalization in **P3** is a more beneficial approach. From the $I-V$ curve in Figure 5, a reduced performance of **P2** compared to **P3** is already evident. The data of Figure 5 can be analyzed by comparison with exciton dissociation models. For this, the photocurrent quantum yield for **P2** and **P3** is plotted as a function of internal electric field in Figure 6. The photocurrent quantum yield has been normalized to unity at the saturation value obtained for high field strengths since, for sufficiently high field, complete exciton dissociation and extraction are obtained.[30] The internal field F is calculated by subtracting the applied voltage from the open-circuit voltage and dividing the result by the active layer thickness of the device. The effect

dx.doi.org/10.1021/jp407014q | J. Phys. Chem. C XXXX, XXX, XXX−XXX

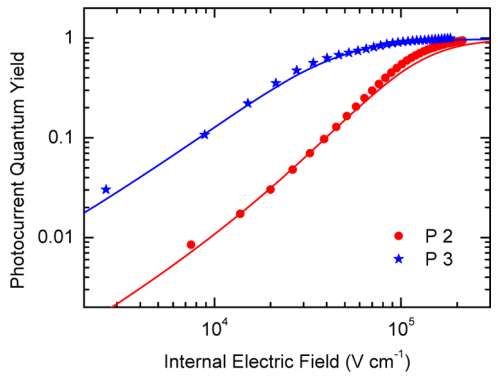

Figure 6. Normalized field-dependent photocurrent quantum yields of copolymer/C_{60} bilayer devices calculated from the photocurrent under AM 1.5 conditions. The lines indicate fits based on an effective mass model that includes interfacial dipole effects.

of possible deviations in the internal field from the value obtained by this method is discussed in detail in ref 31. Figure 6 shows that a higher electrical field is needed to dissociate all excitons in **P2** ($F_{saturation}$ = 1.5 × 10^5 V cm^{-1}) than in **P3** ($F_{saturation}$ = 6 × 10^4 V cm^{-1}), implying that excitons in **P2** are more tightly bound than those in **P3**.

Exciton dissociation at the interface between a polymer donor material and a fullerene acceptor is understood to be assisted by both electrostatic interface effects ("interfacial dipole", parametrized through a fractional dipole strength α) and charge delocalization. The latter can be parametrized in terms of a heuristic "effective mass" of the hole on the polymer.[31] Whereas electrostatic effects screen the mutual coulomb attraction of electron and hole, the kinetic energy associated with a delocalized hole helps its escape from the coulomb potential of its geminate electron.[33−35] In order to obtain insight into the observed photodissociation behavior, we have fitted the field-dependent photocurrent quantum yields with a model containing the effects of both interfacial dipoles and hole delocalization (eqs 3, 6, and 7 in[31]). Good agreement with the experimental data can be obtained when the fractional dipole strength α at the interface to C_{60} is set at 0.050 in **P2** and at 0.045 in **P3**, leading to effective relative hole masses m_{eff}/m_e of 0.44 for **P2** and 0.25 for **P3**, where m_e is the mass of a free electron. These parameter values obtained are consistent with earlier work on homopolymers in bilayers with C_{60}.[31] The fractional dipole strengths are about twice as high as those measured for homopolymer/C_{60} interfaces, and the effective masses are in a similar range, depending on the degree of conjugation of the polymers. As detailed in the Supporting Information, it is possible to increase the fractional dipole strength for **P2** while maintaining a good agreement with the data when simultaneously increasing the hole effective mass further.

What is the insight obtained from these values? This analysis tells us that the improved performance of **P3** compared to **P2**, i.e. the higher photodissociation at low internal field strength, and concomitantly the higher short-circuit current and fill factor, are a result of the lower effective mass in **P3**. A more delocalized character of the hole on **P3** is fully consistent with the overall more delocalized character of the excited state in **P3** that is manifested in the optical measurements, and the higher hole mobility in **P3**. Furthermore, the photocurrent analysis shows a more localized hole on **P2** to be associated with a poor photodissociation, while the CT-character of **P2** does not turn out to be of benefit to the charge separation process. A more localized hole with a higher effective mass derived in the photocurrent fit corresponds well with the reduced hole mobility measured for **P2** in SCLC measurements. The fact that this correlates with a low HOMO level points at trapping effects or localization effects.[36,37] Comparing these results of field-dependent photocurrent quantum yields with previous work on charge separation emphasizes the importance of a good conjugation to facilitate charge separation.

5. CONCLUSION

On comparison of the homopolymer **P1** with the two D−A-copolymers **P2** and **P3**, we could get conclusive information regarding the effective design of D−A-copolymers for an efficient delocalization/conjugation and good charge generation. The introduction of the strong electron withdrawing dicyanovinyl acceptor unit as side chain in **P2** reduces the electron richness and delocalization of the TPA main chain. As a consequence the HOMO level is lowered in **P2** and the hole mobility is decreased. **P2** has a pronounced excited-state CT-character compared to **P3** in which the acceptor enters into delocalization with the backbone. Field-dependent photocurrent measurements in bilayer devices clearly indicate the advantage of the alternating D−A-copolymer strategy in which the donor and acceptor moieties exhibit a better conjugation. Thus, for this material system, charge separation is obtained more readily when the acceptor group is located within the copolymer backbone guaranteeing delocalization along the main chain. The concept of adding a strong acceptor to the side group which lowers the delocalization in the main chain, in contrast, results in a lower hole mobility and stronger bound electron hole pairs and thus lower solar cell power conversion efficiency.

■ ASSOCIATED CONTENT

Ⓢ Supporting Information

Syntheses of the monomers, ^{1}H NMR and FT-IR spectra, cyclic voltammetry data, SCLC curves for different layer thicknesses and corresponding fit parameters, lifetime measurements, and fits with the dipole model and solar cell parameters. This material is available free of charge via the Internet at http://pubs.acs.org.

■ AUTHOR INFORMATION

Corresponding Author

*Phone: +49-921-553108. E-mail: mukundan.thelakkat@uni-bayreuth.de.

Notes

The authors declare no competing financial interest.

■ ACKNOWLEDGMENTS

We acknowledge the Graduate School GRK 1640 of the Deutsche Forschungsgemeinschaft (DFG) and the Bavarian State Ministry of Science, Research, and the Arts for the Collaborative Research Network "Solar Technologies go Hybrid" for financial support and K.N. thanks the Universität Bayern e.V. for financial support in the form of a scholarship of the Bayerische Graduiertenförderung and the Elitenetzwerk Bayern (ENB). We also thank Sabrina Willer for support in the synthesis work and Sebastian Hoffmann and Stephan Kümmel for fruitful discussions.

REFERENCES

(1) Deibel, C.; Dyakonov, V., Polymer-Fullerene Bulk Heterojunction Solar Cells. *Rep. Prog. Phys.* **2010**, *73*.

(2) Green, M. A.; Emery, K.; Hishikawa, Y.; Warta, W.; Dunlop, E. D. Solar Cell Efficiency Tables (Version 40). *Prog. Photovoltaics* **2012**, *20*, 606−614.

(3) Li, Y. Molecular Design of Photovoltaic Materials for Polymer Solar Cells: Toward Suitable Electronic Energy Levels and Broad Absorption. *Acc. Chem. Res.* **2012**, *45*, 723−733.

(4) Boudreault, P. L. T.; Najari, A.; Leclerc, M. Processable Low-Bandgap Polymers for Photovoltaic Applications. *Chem. Mater.* **2011**, *23*, 456−469.

(5) Duan, C. H.; Cai, W. Z.; Huang, F.; Zhang, J.; Wang, M.; Yang, T. B.; Zhong, C. M.; Gong, X.; Cao, Y. Novel Silafluorene-Based Conjugated Polymers with Pendant Acceptor Groups for High Performance Solar Cells. *Macromolecules* **2010**, *43*, 5262−5268.

(6) Hellström, S.; Lindgren, L. J.; Zhou, Y.; Zhang, F. L.; Inganäs, O.; Andersson, M. R. Synthesis and Characterization of Three Small Band Gap Conjugated Polymers for Solar Cell Applications. *Polym. Chem.* **2010**, *1*, 1272−1280.

(7) Hou, J. H.; Tan, Z. A.; Yan, Y.; He, Y. J.; Yang, C. H.; Li, Y. F. Synthesis and Photovoltaic Properties of Two-Dimensional Conjugated Polythiophenes with Bi(thienylenevinylene) Side Chains. *J. Am. Chem. Soc.* **2006**, *128*, 4911−4916.

(8) Zhang, Z. G.; Liu, Y. L.; Yang, Y.; Hou, K. Y.; Peng, B.; Zhao, G. J.; Zhang, M. J.; Guo, X.; Kang, E. T.; Li, Y. F. Alternating Copolymers of Carbazole and Triphenylamine with Conjugated Side Chain Attaching Acceptor Groups Synthesis and Photovoltaic Application. *Macromolecules* **2010**, *43*, 9376−9383.

(9) Zhang, Z.-G.; Wang, J. Structures and Properties of Conjugated Donor-Acceptor Copolymers for Solar Cell Applications. *J. Mater. Chem.* **2012**, *22*, 4178−4187.

(10) Zhang, Z. G.; Zhang, K. L.; Liu, G.; Zhu, C. X.; Neoh, K. G.; Kang, E. T. Triphenylamine-Fluorene Alternating Conjugated Copolymers with Pendant Acceptor Groups: Synthesis, Structure-Property Relationship, and Photovoltaic Application. *Macromolecules* **2009**, *42*, 3104−3111.

(11) Clarke, T. M.; Ballantyne, A.; Shoaee, S.; Soon, Y. W.; Duffy, W.; Heeney, M.; McCulloch, I.; Nelson, J.; Durrant, J. R. Analysis of Charge Photogeneration as a Key Determinant of Photocurrent Density in Polymer: Fullerene Solar Cells. *Adv. Mater.* **2010**, *22*, 5287−5291.

(12) Clarke, T. M.; Durrant, J. R. Charge Photogeneration in Organic Solar Cells. *Chem. Rev.* **2010**, *110*, 6736−6767.

(13) Veldman, D.; Ipek, O.; Meskers, S. C. J.; Sweelssen, J.; Koetse, M. M.; Veenstra, S. C.; Kroon, J. M.; van Bavel, S. S.; Loos, J.; Janssen, R. A. J. Compositional and Electric Field Dependence of the Dissociation of Charge Transfer Excitons in Alternating Polyfluorene Copolymer/Fullerene Blends. *J. Am. Chem. Soc.* **2008**, *130*, 7721−7735.

(14) Tautz, R.; Da Como, E.; Limmer, T.; Feldmann, J.; Egelhaaf, H. J.; von Hauff, E.; Lemaur, V.; Beljonne, D.; Yilmaz, S.; Dumsch, I.; Allard, S.; Scherf, U. Structural Correlations in the Generation of Polaron Pairs in Low-Bandgap Polymers for Photovoltaics. *Nat. Commun.* **2012**, *3*, No. 970.

(15) Carsten, B.; Szarko, J. M.; Son, H. J.; Wang, W.; Lu, L. Y.; He, F.; Rolczynski, B. S.; Lou, S. J.; Chen, L. X.; Yu, L. P. Examining the Effect of the Dipole Moment on Charge Separation in Donor-Acceptor Polymers for Organic Photovoltaic Applications. *J. Am. Chem. Soc.* **2011**, *133*, 20468−20475.

(16) Thelakkat, M. Star-Shaped, Dendrimeric and Polymeric Triarylamines as Photoconductors and Hole Transport Materials for Electro-Optical Applications. *Macromol. Mater. Eng.* **2002**, *287*, 442−461.

(17) Roncali, J. Synthetic Principles for Bandgap Control in Linear Pi-Conjugated Systems. *Chem. Rev.* **1997**, *97*, 173−205.

(18) deMello, J. C.; Wittmann, H. F.; Friend, R. H. An Improved Experimental Determination of External Photoluminescence Quantum Efficiency. *Adv. Mater.* **1997**, *9*, 230−232.

(19) Hong, S. Y.; Marynick, D. S. Understanding the Conformational Stability and Electronic-Structures of Modified Polymers Based on Polythiophene. *Macromolecules* **1992**, *25*, 4652−4657.

(20) Liang, Y. Y.; Feng, D. Q.; Guo, J. C.; Szarko, J. M.; Ray, C.; Chen, L. X.; Yu, L. P. Regioregular Oligomer and Polymer Containing Thieno[3,4-B]thiophene Moiety for Efficient Organic Solar Cells. *Macromolecules* **2009**, *42*, 1091−1098.

(21) Schlüter, A. D. The Tenth Anniversary of Suzuki Polycondensation (Spc). *J. Polym. Sci., Part A: Polym. Chem.* **2001**, *39*, 1533−1556.

(22) Park, J. H.; Seo, Y. G.; Yoon, D. H.; Lee, Y. S.; Lee, S. H.; Pyo, M.; Zong, K. A Concise Synthesis and Electrochemical Behavior of Functionalized Poly(Thieno[3,4-B]Thiophenes): New Conjugated Polymers with Low Bandgap. *Eur. Polym. J.* **2010**, *46*, 1790−1795.

(23) Kun, H.; Yi, H.; Johnson, R. G.; Iraqi, A. Fluoro-Protected Carbazole Main-Chain Polymers as a New Class of Stable Blue Emitting Polymers. *Polym. Adv. Technol.* **2008**, *19*, 299−307.

(24) Noviandri, I.; Brown, K. N.; Fleming, D. S.; Gulyas, P. T.; Lay, P. A.; Masters, A. F.; Phillips, L. The Decamethylferrocenium/Decamethylferrocene Redox Couple: A Superior Redox Standard to the Ferrocenium/Ferrocene Redox Couple for Studying Solvent Effects on the Thermodynamics of Electron Transfer. *J. Phys. Chem. B* **1999**, *103*, 6713−6722.

(25) Gräf, K.; Rahim, M. A.; Das, S.; Thelakkat, M. Complementary Co-Sensitization of an Aggregating Squaraine Dye in Solid-State Dye-Sensitized Solar Cells. *Dyes Pigm.* **2013**, *99*, 1101−1106.

(26) Goh, C.; Kline, R. J.; McGehee, M. D.; Kadnikova, E. N.; Fréchet, J. M. J. Molecular-Weight-Dependent Mobilities in Regioregular Poly(3-Hexyl-thiophene) Diodes. *Appl. Phys. Lett.* **2005**, *86*, No. 122110.

(27) Meskers, S. C. J.; Hübner, J.; Oestreich, M.; Bässler, H. Dispersive Relaxation Dynamics of Photoexcitations in a Polyfluorene Film Involving Energy Transfer: Experiment and Monte Carlo Simulations. *J. Phys. Chem. B* **2001**, *105*, 9139−9149.

(28) Tress, W.; Petrich, A.; Hummert, M.; Hein, M.; Leo, K.; Riede, M. Imbalanced Mobilities Causing S-Shaped IV Curves in Planar Heterojunction Organic Solar Cells. *Appl. Phys. Lett.* **2011**, *98*, No. 063301.

(29) Carsten, B.; Szarko, J. M.; Lu, L. Y.; Son, H. J.; He, F.; Botros, Y. Y.; Chen, L. X.; Yu, L. P. Mediating Solar Cell Performance by Controlling the Internal Dipole Change in Organic Photovoltaic Polymers. *Macromolecules* **2012**, *45*, 6390−6395.

(30) Schwarz, C.; Bässler, H.; Bauer, I.; Koenen, J. M.; Preis, E.; Scherf, U.; Köhler, A. Does Conjugation Help Exciton Dissociation? A Study on Poly(*p*-Phenylene)s in Planar Heterojunctions with C_{60} or TNF. *Adv. Mater.* **2012**, *24*, 922−925.

(31) Schwarz, C.; Tscheuschner, S.; Frisch, J.; Winkler, S.; Koch, N.; Bässler, H.; Köhler, A. Role of the Effective Mass and Interfacial Dipoles on Exciton Dissociation in Organic Donor-Acceptor Solar Cells. *Phys. Rev. B* **2013**, *87*, No. 155205.

(32) Verlaak, S.; Beljonne, D.; Cheyns, D.; Rolin, C.; Linares, M.; Castet, F.; Cornil, J.; Heremans, P. Electronic Structure and Geminate Pair Energetics at Organic-Organic Interfaces: The Case of Pentacene/C-60 Heterojunctions. *Adv. Funct. Mater.* **2009**, *19*, 3809−3814.

(33) Arkhipov, V. I.; Heremans, P.; Bässler, H. Why Is Exciton Dissociation So Efficient at the Interface between a Conjugated Polymer and an Electron Acceptor? *Appl. Phys. Lett.* **2003**, *82*, 4605−4607.

(34) Nenashev, A. V.; Baranovskii, S. D.; Wiemer, M.; Jansson, F.; Österbacka, R.; Dvurechenskii, A. V.; Gebhard, F. Theory of Exciton Dissociation at the Interface between a Conjugated Polymer and an Electron Acceptor. *Phys. Rev. B* **2011**, *84*, No. 035210.

(35) Wiemer, M.; Nenashev, A. V.; Jansson, F.; Baranovskii, S. D. On the Efficiency of Exciton Dissociation at the Interface between a Conjugated Polymer and an Electron Acceptor. *Appl. Phys. Lett.* **2011**, *99*, No. 013302.

(36) Nicolai, H. T.; Kuik, M.; Wetzelaer, G. A. H.; de Boer, B.; Campbell, C.; Risko, C.; Brédas, J. L.; Blom, P. W. M. Unification of

Trap-Limited Electron Transport in Semiconducting Polymers. *Nat. Mater.* **2012**, *11*, 882−887.
(37) Hoffmann, S. T.; Jaiser, F.; Hayer, A.; Bässler, H.; Unger, T.; Athanasopoulos, S.; Neher, D.; Köhler, A. How Do Disorder, Reorganization, and Localization Influence the Hole Mobility in Conjugated Copolymers. *J. Am. Chem. Soc.* **2013**, *135*, 1772−1782.